crystals

MDPI

Article

Optical Temperature Sensor Capabilities of the Green Upconverted Luminescence of Er^{3+} in La_3NbO_7 Ceramic Powders

Miguel A. Hernández-Rodríguez [1], Alvaro Egaña [2], Ulises R. Rodríguez-Mendoza [3], Victor Lavín [3] and Juan E. Muñoz-Santiuste [2,*]

[1] Phantom-G, CICECO—Aveiro Institute of Materials, Department of Physics, Universidade de Aveiro, 3810-193 Aveiro, Portugal; miguelandreshr@gmail.com
[2] Departamento de Física, MALTA Consolider Team, Escuela Politécnica Superior, Universidad Carlos III de Madrid, Avenida de la Universidad 30, E-28911 Leganés, Madrid, Spain; alvega08@gmail.com
[3] Departamento de Física, MALTA Consolider Team, IMN and IUdEA, Universidad de La Laguna, Apdo. 456, E-38200 San Cristóbal de La Laguna, Santa Cruz de Tenerife, Spain; urguez@ull.edu.es (U.R.R.-M.); vlavin@ull.edu.es (V.L.)
* Correspondence: jems@fis.uc3m.es

Abstract: We present a study of the Er^{3+} upconverted luminescence in erbium doped Lanthanum Niobium Oxide, La_3NbO_7, ceramic powder, prepared by solid state reaction. This study focuses on the analysis of the feasibility of this system as a temperature sensor. Efficient UC luminescence was observed under the 975 nm excitation showing intense green, red and NIR (850 nm) emission bands. The NIR luminescence centred at about 850 nm and lying on the first biological window is mainly insensitive to the temperature. In contrast, the upconverted green bands, associated with the $(^2H_{11/2}, ^4S_{3/2}) \rightarrow ^4I_{15/2}$ transitions, showed a high sensibility to temperature. Their temperature dependence was studied from RT up to 525 K, paying special attention to the physiological range of temperature (303–318 K). The high thermal sensitivities obtained, in comparison with other Er^{3+} and Er^{3+}-Yb^{3+} based optical temperature sensors in such ranges, suggest the potential application of this phosphor in thermal sensing, suitable for both biological systems and other industrial applications requiring higher temperatures.

Keywords: fluorescence intensity ratio; optical temperature sensor; Er^{3+}; up-conversion luminescence; sensitivity

Citation: Hernández-Rodríguez, M.A.; Egaña, A.; Rodríguez-Mendoza, U.R.; Lavín, V.; Muñoz-Santiuste, J.E. Optical Temperature Sensor Capabilities of the Green Upconverted Luminescence of Er^{3+} in La_3NbO_7 Ceramic Powders. *Crystals* **2022**, *12*, 455. https://doi.org/10.3390/cryst12040455

Academic Editor: Jesús Sanmartín-Matalobos

Received: 28 February 2022
Accepted: 22 March 2022
Published: 24 March 2022

1. Introduction

Measuring temperature accurately and reliably is very important in several application areas, ranging from health care to industrial applications [1–5]. The working mechanism of optical temperature sensors is based on the temperature dependence of the material's optical properties, which allows for the monitoring of temperature in certain locations such as in electrical power stations, refineries, and coal mines. These sensors can also be useful in building fire detection [6,7]. In addition to precision and reliability, other characteristics such as high sensitivity and resolution and fast response are also required when using these materials as temperature sensors [2]. Changes in optical properties and their dependence on temperature have been studied in different ways: the spectral position of emission and absorption lines, their intensity, bandwidths and decay time and even polarization [2]. Since the discussions in the 1970s of the possible application of the fluorescence intensity ratio (FIR) technique for temperature sensing [8], this technique is among the most widely used due to its excellent advantages in terms of sensitivity and stability [9]. The classical use of this technique requires the presence of thermally coupled levels (TCL), two nearby energy levels which are assumed to be in a state of thermal quasi-equilibrium [10], in which luminescence intensities are measured. The energy distance

between these TCLs must be small enough to allow a redistribution of the population of thermal origin between the lower and higher energy levels, which is the origin of the FIR technique. However, at the same time there has to be a separation between levels large enough to solve the emission lines originating in each one of them. A typical value between 200 and 2000 cm^{-1} [11] is usually accepted as the energy gap between levels that allows the application of the FIR technique. Most of the trivalent lanthanide ions (Pr^{3+}, Nd^{3+}, Eu^{3+}, Ho^{3+}, Er^{3+}, Tm^{3+}) fulfil the above requirement and their introduction in small amounts into host materials of different types allows for the use of these materials as potential optical thermometers [12–16]. The narrow absorption and emission bands and the relatively long luminescence lifetimes commonly observed in trivalent lanthanide ions are the principal advantages of these materials compared to other organic materials and quantum dots. Furthermore, the specific properties of the various host materials make it possible to configure rare-earth doped systems providing a wide variety of additional advantages. For instance, we highlight the high resistance to blinking or photobleaching of some materials, allowing wide applications in forensic sciences, biomedicine (bioimaging, photo-dynamic therapy or laser heating), optical temperature and/or pressure sensors [15–20].

Oxides with general formula La_3BO_7 (B = Os, Re, Nb, Ta and other transition metals) manifest some interesting catalytic, dielectric and magnetic properties [21–23]. Due to their comparatively high melting points, fine particle size, chemical stability and proton conductivity at high temperatures, La_3TaO_7 and La_3NbO_7 are proposed as materials for thermal barrier coatings [24] or as electrolytes [25,26] in some high temperature electrolysers. The weberite like structure of La_3NbO_7 compounds is an anion-deficient fluorite-related superstructure with *Cmcm* space group [27]. The structure is usually described as formed by slabs of c-axis oriented chains of tilted NbO_6 octahedra, sharing corners with parallel rows of lanthanum dodecahedra (one third of La ions in 8-fold oxygen coordination) edge-sharing parallel to (100). The remaining La ions, having 7-fold oxygen coordination, lie in between these layers. La ions can be substituted by other rare earth (RE) ions of similar radius.

In a previous work [28], we report the optical properties of the Er^{3+}-doped La_3NbO_7 ceramic compound, checking the properties of this system from a structural point of view; we consider the viability of incorporating luminescent ions in this matrix and the effect of the impurities on the structure, etc., through the erbium luminescence. In this work, we explore the capabilities of the upconverted green emission of phosphors $La_{3-}NbO_7$:Er^{3+} as an optical temperature sensor working in the VIS range, under NIR excitation for two different temperature ranges: those with applications in biological processes (303–318 K) and biomedicine and in other higher temperature ranges (up to 525 K) relevant for industrial applications.

2. Materials and Methods

Following the synthesis route described in Reference [29], we prepared powder samples with nominal composition $La_{3-x}Er_xNbO_7$ (x = 0.01, 0.05 and 0.1) by the solid state reaction method. Stochiometric amounts of La_2O_3 (99.99%), Er_2O_3 (99.9%) and Nb_2O_5 (99.9%) Sigma-Aldrich (Darmstadt, Germany) powders were used as precursor. Rietveld's analysis was carried out for X-ray diffraction patterns obtained from the samples confirmed by the orthorhombic *Cmcm* space group where the erbium ions were randomly allocated in the lanthanum sites 4c and 8g, surrounded by 8 and 7 oxygens, respectively. The X-ray diffraction patterns of a series of sintered samples with increasing amounts of Er_2O_3 powders previously reported in [28] prove the formation of the $La_{3-x}Er_xNbO_7$ phase (x = 0.01, 0.05, 0.1), with the largest peaks indexed with the type structure weberite based on the *Cmcm* space group. However, (see Supplementary Materials), some additional peaks appear in the XRD patterns and the foreign reflections correspond to a small amount of $LaNbO_4$ secondary phase. The relative percentage of this secondary phase increases with the amount of erbium in the samples. This fact appears to be inherent to the fabrication route in which the presence of Er^{3+} disturbs the necessary secondary

$La_2O_3 + LaNbO_4 \rightarrow La_3NbO_7$ reaction and eventually becomes responsible for the segregated phases [28,29]. Samples of the nominal formula $La_{3-x}Er_xNbO_7$ (x = 0.1), having 9.6% of $LaNbO_4$ secondary phase, were used in this work in an effort to maximize the emission intensity. Although present in our samples, the mentioned minority phases do not play a relevant role in our study. Additional details of sample preparation and structural analysis were described in Reference [28], together with the room temperature study of the luminescence of the Er^{3+} ion in this host matrix.

Up-conversion luminescence experiments presented in this work were performed in the temperature range from RT to 525 K in a tube-shaped electric furnace with the sample placed in its centre. The heating rate was 1 K/min to maintain thermal stability in the sample. The furnace temperature was monitored with a K-type thermocouple positioned close to the sample and connected to a voltmeter Fluke Calibrator 714 (Fluke Calibration, Everett, WA, USA). Erbium up-converted luminescence was excited using a tunable Ti-sapphire cw laser Spectra Physics 3900S (Fluke Calibration, Everett, WA, USA) pumped by a 532 nm diode laser (Spectra Physics Millennia Prime Laser 15SJSPG). The excitation wavelength was selected to be 975 nm. To avoid overheating the sample, the laser power was kept as low as possible. Through a lens system at the furnace exit, the up-converted green emissions were collimated and then focused on an optical fiber coupled to a 0.3 m focal length single grating spectrometer (Andor Shamrock 303i). The light was detected by a Peltier cooled silicon CCD camera (Andor Newton DU490A-1.7) with a resolution of about 0.7 nm (about 25 cm^{-1} in the green region) and an integration time of 10 s. All spectra were corrected for the spectral response of the equipment. Conventional room temperature luminescence measurements were performed using a 488–490 nm laser diode as an excitation source and emission signal was detected with the experimental set-up described elsewhere [28].

Fluorescence Intensity Ratio (FIR) Technique

FIR technique uses the ratio between the intensities of the emissions coming from two TCL to characterize a temperature sensor in the following way [9]. Consider the luminescence of two TCL, having E_1 and E_2 energies, to a final level with energy E_0 (see Figure 1) being I_{20} and I_{10} their respective integrated intensities. By describing the population of both levels in thermal equilibrium using Boltzmann's distribution, we can define a thermometric parameter Δ as [9]:

$$\Delta = \frac{I_{20}}{I_{10}} = \frac{\omega_{20}^{R} g_2 E_2}{\omega_{10}^{R} g_1 E_1} e^{-E_{21}/KT} = C\, e^{-E_{21}/KT} \quad (1)$$

where K is the Boltzmann constant, $E_{21} = E_2 - E_1$ is the energy separation between the thermalized emitter levels, g_2 and g_1 their respective degenerations (2J + 1) and ω_{ij}^{R} is the spontaneous emission rates that can be calculated using the theory of Judd–Ofelt [30–34]. Besides accuracy, two relevant figure quantities characterize a thermal sensor: the relative sensitivity and the resolution. The sensor relative thermal sensitivity S_{REL} (in % K^{-1}) is defined using the following expression [35]:

$$S_{REL} = \frac{1}{\Delta}\left|\frac{d\Delta}{dT}\right| \times 100 = \left(\frac{E_{21}}{KT^2}\right) \times 100 \quad (2)$$

This parameter has the advantage of allowing the comparison of the performance with temperature of different optical temperature sensors regardless of their nature. From Equation (2), larger energy gap between the TCL levels implies higher thermal sensitivity. Nonetheless, this is true only to a certain extent, because larger energy gap also means lower population in the upper level, leading to lower intensity emission coming from such level [9,35].

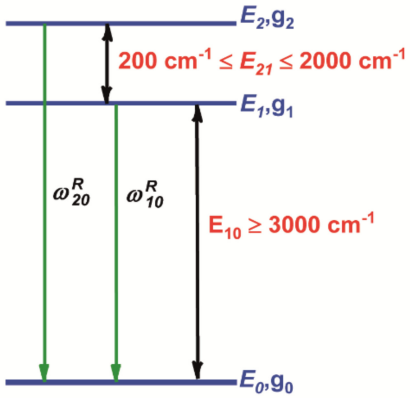

Figure 1. Simple scheme for thermal coupled energy levels theory. E_{21} is the energy gap between the two excited levels E_2 and E_1, g_i is the degeneracy of the i-th level and ω_{ij}^R is the spontaneous emission rate between the i-th and j-th levels.

Concerning the temperature resolution, it is usual to define the temperature uncertainty, δT (in K), as the smallest temperature change that can be achieved in each measurement. The temperature uncertainty can be estimated according to the equation: [35]:

$$\delta T = \frac{1}{S_{REL}} \frac{\delta \Delta}{\Delta} \quad (3)$$

where S_{REL} is the relative sensitivity and the $\delta\Delta/\Delta$ is the relative uncertainty on Δ, which for typical sensitive detectors (CCDs, among others) is around 0.03% [35].

3. Results and Discussion

3.1. Luminescence

VIS-NIR conventional luminescence of Er^{3+} ions obtained from a $La_{2.9}Er_{0.1}NbO_7$ powder sample excited at 488 nm and the upconverted luminescence obtained under the 975 nm excitation, both recorded in ambient conditions, are shown in Figure 2. A simplified level scheme is included on the side of Figure 2 showing the main excitation channels in which these VIS-NIR emissions are originated. In the VIS region, we observe the characteristic green bands corresponding to the ($^2H_{11/2}$,$^4S_{3/2}$) → $^4I_{15/2}$, transitions, dominating the spectra, together with a less intense red emission band centred at 660 nm corresponding to the $^4F_{9/2}$→$^4I_{15/2}$ erbium transition. A low NIR luminescence band centred at about 850 nm, lying on the first biological window and corresponding to the $^4S_{3/2}$ → $^4I_{13/2}$ transition, is also obtained. From the analysis of integrated intensity of upconverted emission versus excitation power, a slope of 1.5 is obtained (see inset in the lower side), indicating that at least two IR photons are involved in the process in accordance with previous data [28,36,37]. We must note that the same bands are obtained in both spectra, but they have different relative intensities, depending on the luminescence origin. Obviously, the spectrum at the bottom of this figure was not obtained with low-power laser excitation. Thus, the effective temperature of the sample is higher in this spectrum than in that of conventional luminescence (upper side of the figure), originating from the 530 nm band having higher relative intensity. In all luminescence channels, the luminescence consists of broad bands, formed by a strong spread of narrow lines that extend to energies lower than usual values in other oxides. This fact is indicative of the Er^{3+} incorporation in a system with occupation of several available centres. Indeed, some intense narrow emission peaks observed in the low energy side of each emission band, those centred at 573, 695 and 883 nm, appear as characteristic features of the Er^{3+} luminescence in these samples. As the La_3NbO_7 matrix has two La sites with different oxygen coordination, we can assume that this widespread characteristic luminescence is mainly due to the emission of erbium ions incorporated in both sites, as was previously indicated [28]. However, because samples

are fine powders in which the discontinuity in grain boundaries supports several types of defects, and due to the presence of $LaNbO_4$ secondary phase in the samples used in this work, the origin of the emission peaks is not definitively clear. Finally, we must emphasize that the presence of the secondary $LaNbO_4$ phase does not seem to play a significant role in this study, since we have not found differences in the luminescence behaviour in samples with different erbium concentration $La_{3-x}NbEr_xO_7$ with x = 0.01, 0.05 or 0.1) nor in samples with the same erbium nominal concentration (x = 0.1) synthesized in different series; so, the measurements' repeatability appears to be guaranteed.

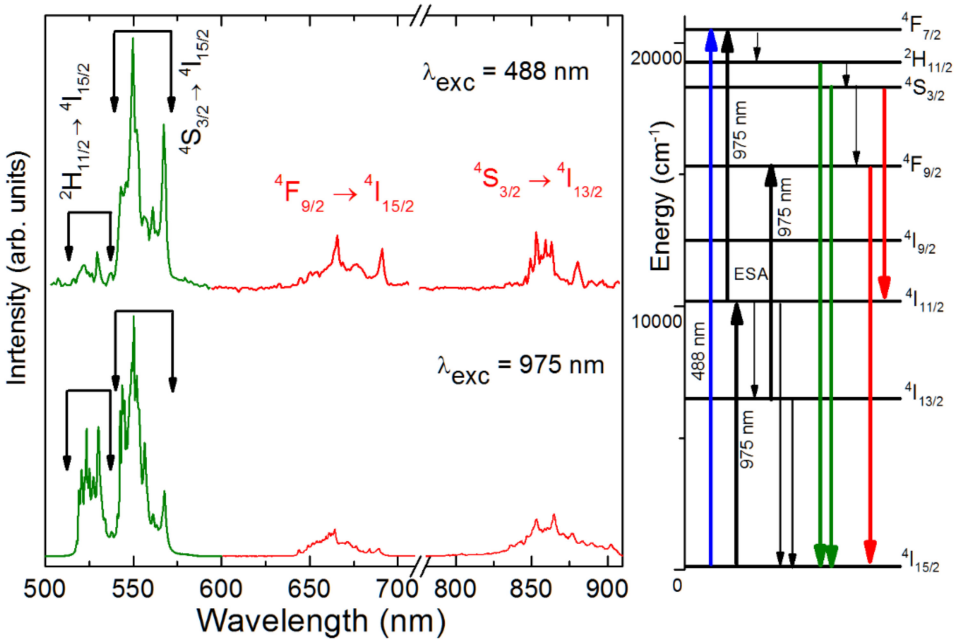

Figure 2. Luminescence spectrum of the phosphor with nominal composition $La_{2.9}Er_{0.1}NbO_7$ obtained at ambient conditions under 488 nm (upper) and under 975 nm laser excitation (lower). Main transitions are indicated in the upper spectrum. On the right side, a simplified level scheme of Er^{3+} ion is sketched showing the excitation and de-excitation channels. The inset in the lower spectra shows an example of the upconverted intensity versus excitation power obtained for the emission at 850 nm, showing a slope of 1.5. Similar results were previously reported for green and red upconverted bands [28].

3.2. Optical Sensor Calibration

We have studied the temperature dependence of all upconverted emission bands. Concerning the ~850 nm NIR luminescence lying on the first biological window, our primary interest was focused on the physiological range of temperature (303–318 K). Unfortunately, we found that both intensity and shape of the 850 nm band are mainly insensitive to the temperature changes in this narrow range of temperature.

Since the green upconverted emissions of $La_{3-x}NbO_7$: Er^{3+} (x = 0.1) phosphor present high intensities and quantum yields along with the hypersensitivity of the upper thermalized energy level $^2H_{11/2}$ [30,38], we analysed the feasibility of using this powdered material as a temperature sensor, working not only in the VIS range belonging within the physiological range of temperature but also at high temperatures.

In this regard, the temperature evolution of the green upconverted emissions related to the ($^2H_{11/2}$,$^4S_{3/2}$) → $^4I_{15/2}$ transitions of Er^{3+} ions were measured in this sample, and the obtained spectra are shown in Figure 3. In these spectra it can be observed that as the temperature increases, the intensity of the emission band related to the transition $^2H_{11/2}$→ $^4I_{15/2}$ also increases. In addition, the $^4S_{3/2}$ → $^4I_{15/2}$ emission band decreases due to the thermally induced population from this level to the upper one. In this sense, the relationship between the intensity areas of these green upconverted emission bands

related to the $(^2H_{11/2}, ^4S_{3/2}) \rightarrow {}^4I_{15/2}$ can be considered as I_{20} and I_{10} in order to obtain the "upconverted" radiometric thermometric Δ in Equation (2).

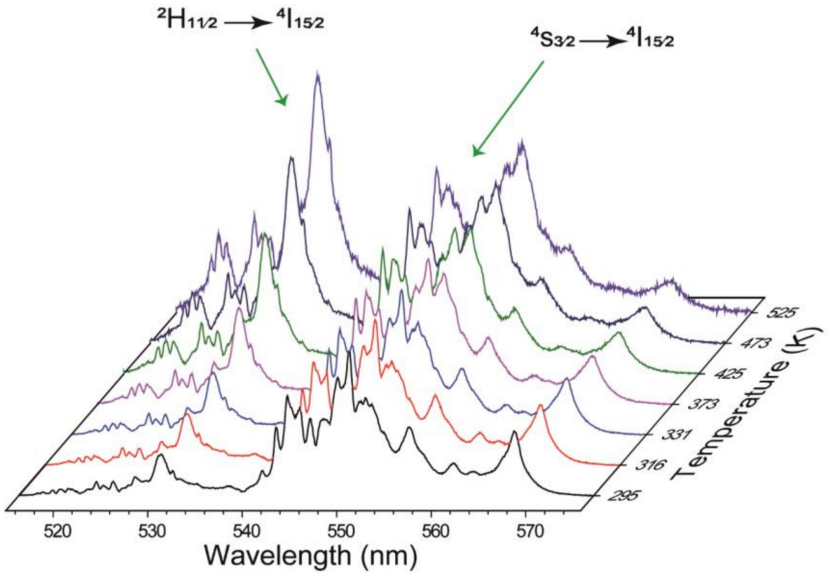

Figure 3. Thermal evolution of the normalized green upconverted emissions of $La_{2.9}Er_{0.1}NbO_7$ phosphor from 295 K up to 525 K under 975 nm laser excitation.

The temperature evolution of Δ in the whole range of temperature is shown in Figure 4. It is clearly observed that such parameter increases as the temperature does, describing a curve that can be simulated using the Boltzmann's distribution law (Equation (1)). Using a standard least-squares fitting procedure, the values of C = 5.96 and an energy gap E_{21} = 768 cm^{-1} were determined. This data and the high thermal stability of this compound make it to be a good candidate for optical measurements of temperature in a range wider than that studied here.

Let us now focus our attention on the low temperature side of the range studied in this work. The relative thermal sensitivity S_{REL} as a function of temperature T, as defined by Equation (2) and also shown in Figure 4 in the biological range of temperatures, shows relatively high values of around 1.26 and 1.19 % K^{-1} at 295 K and 303 K, respectively, with a low temperature uncertainties δT of around 0.05 K. The capabilities of the $La_{2.9}Er_{0.1}NbO_7$ phosphor as an optical temperature sensor are compared to other Er^{3+} and Er^{3+}-Yb^{3+}-based optical temperature sensors listed in Table 1. From this table, it is clear that this material presents good performance with temperature showing high thermal sensitivities compared to other phosphors, for instance $CaWO_4$:Er^{3+}-Yb^{3+}, $Na_2Y_2B_2O_7$:Er^{3+}-Yb^{3+}, $BaMoO_4$:Er^{3+}-Yb^{3+} or $KLa(MoO_4)_2$:Er^{3+}-Yb^{3+} phosphors [39–42], among others, at high temperature range. On the other hand, $La_{3-x}NbO_7Er_x$ (x = 0.1) phosphor also shows high thermal sensitivities within the physiological temperature range. In this narrow range (303–318 K), the sensitivity is comparable to other materials reported for applications in such range; for example, YAP: Er^{3+}-Yb^{3+} nanoperovskites [13], which also exhibit applications in laser heating, or $NaYbF_4$:Er^{3+} powders [43], which can be used for biological purposes, such as photo-thermal therapy or even drug release.

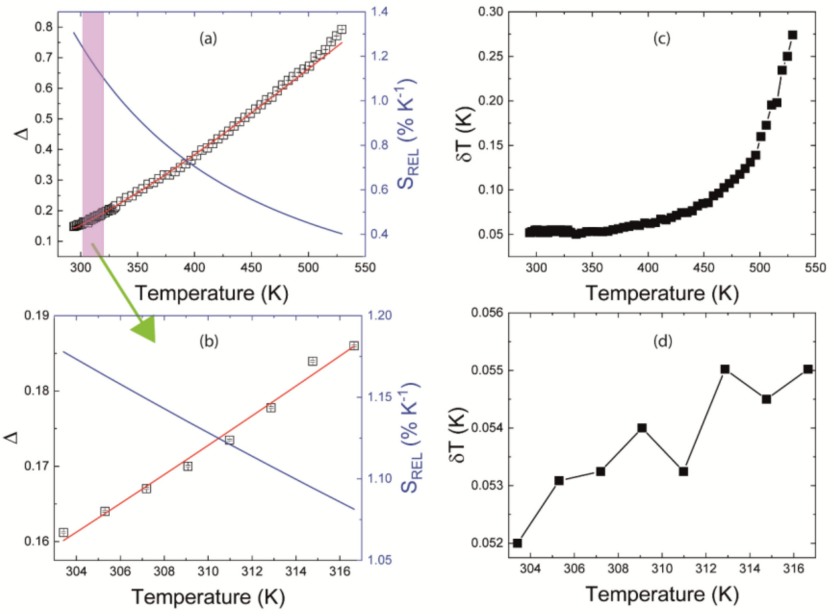

Figure 4. Experimental integrated intensity ratio, Δ, (**a**) in the whole temperature range and (**b**) in the physiological range of temperature (303 K–318 K), black squares, and relative sensitivity (S_{REL}), blue lines of the $La_{2.9}Er_{0.1}NbO_7$ powder samples obtained from the emission bands associated to the $^2H_{11/2} \rightarrow {}^4I_{15/2}$ and $^4S_{3/2} \rightarrow {}^4I_{15/2}$ transitions. A Boltzmann type curve was fitted to the experimental values of Δ according to Equation (1) (red line). Temperature uncertainty, δT, computed by Equation (3) in the (**c**) whole temperature range as well as (**d**) within the physiological range of temperature.

Table 1. Relative S_{REL} thermal sensitivities, temperature range and excitation wavelength of different nanomaterials doped with Er^{3+} ions, or co-doped with Yb^{3+} ions, used in optical temperature sensing in the biological temperature range. Classification has been done according to the value of the relative sensitivity S_R calculated at 303 K.

Er^{3+} Doped and Er^{3+}-Yb^{3+} Based Host Matrix	λ_{exc} (nm)	T Range (K)	FIR Equation	S_{REL} (%K^{-1}) at 303 K	Ref.
BZT-BCT: Er^{3+} ceramic	980	200–443	9.97•exp(−1135/T)	1.24	[44]
Y_2O_3: Er^{3+}-Yb^{3+} nanoparticles	980	273–480	13.30•exp(−1131/T)	1.23	[45]
$ZnMoO_4$:Yb^{3+}-Er^{3+}-Li^+	980	300–400	14.27•exp(−1111/T)	1.21	[46]
$NaYbF_4$: Er^{3+}	980	293–593	10.78•exp(−1098/T)	1.20	[43]
$La_{3-x}NbO_7$: xEr^{3+} (x = 0.1) phosphor	975	295–525	5.96•exp(−1097/T)	1.19	This work
$KLa(MoO_4)_2$: Yb^{3+}-Er^{3+} phosphor	980	303–423	21.95•exp(−1079/T)	1.18	[42]
YAP: Er^{3+}-Yb^3 nanoperovskites	980	296–600	5.77•exp(−1073/T)	1.17	[13]
$Y_3Ga_5O_{12}$: Er^{3+} nanoparticles	488/800	300–335	11.04•exp(−1047/T)	1.16	[47]
$NaYF_4$: Er^{3+}-Yb^{3+} nanocrystals	980	303–483	30.80•exp(−1034/T)	1.13	[48]
$BaMoO_4$: Er^{3+}-Yb^{3+} phosphors	980	300–575	20.06•exp(−980/T)	1.07	[41]
Tellurite glass: Er^{3+}-Yb^3 (7.5 mol% TiO_2)	785	318–431	8.10•exp(−962/T)	1.05	[49]
$CaWO_4$: Er^{3+}-Yb^{3+} phosphors	980	303–753	17.20•exp(−944/T)	1.02	[39]
Chalcogenide glass: Er^{3+}-Yb^3	1060	296–438	8.85•exp(−962/T)	1.01	[7]
$Na_{0.5}Bi_{0.5}TiO_3$: Er^{3+}-Yb^{3+} ceramic	980	93–613	4.71•exp(−827/T)	0.90	[50]
$Na_2Y_2B_2O_7$: Er^{3+}-Yb^{3+} phosphor	980	300–613	27.60•exp(−766/T)	0.83	[40]
$NaLuF_4$:Yb^{3+}-Er^{3+}-Ho^{3+}	975	298–503	1.46•exp(−654/T)	0.71	[14]
Silicate glass: Er^{3+}-Yb^{3+}	980	296–723	3.65•exp(−593/T)	0.64	[51]

The obtained SREL values suggest the application of this material as an optical temperature sensor working in the VIS range, and the obtained parameters suggest that this material is not only interesting from the point of view of industry applications at high temperatures but also within the physiological range of temperature for applications in biological systems.

4. Conclusions

The temperature dependence of green-upconverted emissions of Er^{3+} ions in La_3NbO_7 phosphors was studied within both the physiological temperature range from 303 K to 318 K and at higher temperatures, up to 525 K, under excitation at 975 nm. The thermal sensitivity obtained for the green thermally coupled emission bands ranged between 1.26% K^{-1} at 295 K and 1.19% K^{-1} at 303 K. Compared to other optical temperature sensors based on Er^{3+} and Yb^{3+}-Er^{3+} excited in the NIR range and working in the VIS range, these values are high enough to support the viability of the Er^{3+}:La_3NbO_7 phosphor as an optical temperature sensor. Based on the FIR technique for both temperature ranges under study, the physiological temperature range with applications in biological systems and higher temperature ranges could be interesting for some industrial applications.

Supplementary Materials: The following supporting information can be downloaded at: https://www.mdpi.com/article/10.3390/cryst12040455/s1, Figure S1. Powder XRD pattern of a $La_{3-x}Er_xNbO_7$ (x = 0.1) powder sample. Vertical bars correspond to Bragg positions. Difference between measured and calculated intensities is given at the bottom. Inset shows the high intensity region (25–35 degrees) in which some extra peaks corresponding to the secondary $LaNbO_4$ phase are indicated with "*". The peak marked with "+" is due to La_2O_3, Figure S2. High resolution SEM image (BSE, 5000×) of a region of a $La_{2.9}Er_{0.1}NbO_7$ sample showing regions labeled as A and B with strong microstructure differences. EDS spectra corresponding to (A) and (B) regions are showed in the lower side. Table S1. Structure Refinement Results of $La_{3-x}Er_xNbO_7$ (x = 0.1) from XRD data, Table S2. Results of compositional analysis of regions (A) and (B) from EDS data.

Author Contributions: Conceptualization, M.A.H.-R., V.L., U.R.R.-M. and J.E.M.-S., validation M.A.H.-R., V.L., U.R.R.-M. and J.E.M.-S.; investigation, M.A.H.-R. and A.E.; writing—original draft preparation, M.A.H.-R. and A.E.; writing—review and editing, J.E.M.-S.; supervision, U.R.R.-M., V.L. and J.E.M.-S.; funding acquisition, V.L., U.R.R.-M. and J.E.M.-S. All authors have read and agreed to the published version of the manuscript.

Funding: This research has been partially supported by the Spanish Ministerio de Ciencia, Innovación y Universidades (MICINN) through the Spanish projects RTI2018-101020-B-100 and PID2019-106383GB-C44, by the Madrid Government (Comunidad de Madrid-Spain) under the Multiannual Agreement with UC3M in the line of Excellence of University Professors (EPUC3MXX) and in the context of the V PRICIT (Regional Programme of Research and Technological Innovation) by the Agencia Canaria de Investigación, Innovación y Sociedad de la Información (ACIISI) (ProID2017010078).

Institutional Review Board Statement: Not applicable.

Informed Consent Statement: Not applicable.

Data Availability Statement: Not applicable.

Acknowledgments: M.A.H.-R. thanks MINECO for the FPI grant (BES-2014-068666). U.R.R.-M. thanks Gobierno de Canarias and EU-FEDER for grant ProID2020010067.

Conflicts of Interest: The authors declare no conflict of interest.

References

1. Xu, W.; Cui, Y.; Hu, Y.; Zheng, L.; Zhang, Z.; Cao, W. Optical temperature sensing in Er^{3+}-Yb^{3+} codoped $CaWO_4$ and the laser induced heating effect on the luminescence intensity saturation. *J. Alloy. Compd.* **2017**, *726*, 547–555. [CrossRef]
2. Jaque, D.; Vetrone, F. Luminescence nanothermometry. *Nanoscale* **2012**, *4*, 4301–4326. [CrossRef] [PubMed]
3. Brites, C.D.S.; Lima, P.P.; Silva, N.J.O.; Millán, A.; Amaral, V.S.; Palacio, F.; Carlos, L.D. Thermometry at the nanoscale using lanthanide-containing organic-inorganic hybrid materials. *J. Lumin.* **2013**, *133*, 230–232. [CrossRef]

4. McLaurin, E.; Bradshaw, L.R.; Gamelin, D.R. Dual-Emitting Nanoscale Temperature Sensors. *Chem. Mater.* **2013**, *25*, 1283–1292. [CrossRef]
5. Vetrone, F.; Naccache, R.; Zamarron, A.; de la Fuente, A.J.; Sanz-Rodriguez, F.; Maestro, L.M.; Rodriguez, E.M.; Jaque, D.; García Solé, J.; Capobianco, J.A. Temperature sensing using fluorescent nanothermometers. *ACS Nano* **2010**, *4*, 3254–3258. [CrossRef]
6. Sun, M.; He, Q.; Kuang, X.; Zhang, Q.; Ye, S.; Huang, B. Probing oxide-ion conduction in low-temperature SOFCs. *Nano Energy* **2018**, *50*, 88–96. [CrossRef]
7. Dos Santos, P.V.; De Araujo, M.T.; Gouveia-Neto, A.S.; Medeiros Neto, J.A.; Sombra, A.S.B. Optical temperature sensing using upconversion fluorescence emission in Er^{3+}/Yb^{3+}-codoped chalcogenide glass. *Appl. Phys. Lett.* **1998**, *73*, 578–580. [CrossRef]
8. Kusama, H.; Sovers, O.J.; Yoshioka, T. Line Shift Method for Phosphor Temperature Measurements. *Jpn. J. Appl. Phys.* **1976**, *15*, 2349–2358. [CrossRef]
9. Wade, S.; Collins, S.F.; Baxter, G. Fluorescence intensity ratio technique for optical fiber point temperature sensing. *J. Appl. Phys.* **2003**, *94*, 4743–4756. [CrossRef]
10. Alencar, M.A.R.C.; Maciel, G.S.; de Araújo, C.B.; Patra, A. Er^{3+}-doped $BaTiO_3$ nanocrystals for thermometry: Influence of nanoenvironment on the sensitivity of a fluorescence based temperature sensor. *Appl. Phys. Lett.* **2004**, *84*, 4753–4755. [CrossRef]
11. León-Luis, S.F.; Rodriguez-Mendoza, U.; Lalla, E.; Lavín, V. Temperature sensor based on the Er^{3+} green upconverted emission in a fluorotellurite glass. *Sens. Actuators B Chem.* **2011**, *158*, 208–213. [CrossRef]
12. Hernández-Rodríguez, M.A.; Lozano-Gorrín, A.D.; Martín, I.R.; Rodríguez-Mendoza, U.R.; Lavín, V. Comparison of the sensitivity as optical temperature sensor of nano-perovskite doped with Nd^{3+} ions in the first and second biological windows. *Sens. Actuators B Chem.* **2018**, *255*, 970–976. [CrossRef]
13. Hernández-Rodriguez, M.A.; Lozano-Gorrín, A.D.; Lavín, V.; Rodríguez-Mendoza, U.R.; Martín, I.R.; Manjón, F.J. Analysis of the upconversion emission of yttrium orthoaluminate nano-perovskite co-doped with Er^{3+}/Yb^{3+}ions for thermal sensing applications. *J. Lumin.* **2018**, *202*, 316–321. [CrossRef]
14. Runowski, M.; Bartkowiak, A.; Majewska, M.; Martin, I.R.; Lis, S. Upconverting lanthanide doped fluoride NaLuF4:Yb^{3+}-Er^{3+}-Ho^{3+}-optical sensor for multi-range fluorescence intensity ratio (FIR) thermometry in visible and NIR regions. *J. Lumin.* **2018**, *201*, 104–109. [CrossRef]
15. Hernández-Rodríguez, M.A.; Lozano-Gorrín, A.D.; Lavín, V.; Rodríguez-Mendoza, U.R.; Martín, I.R. Yttrium orthoaluminate nanoperovskite doped with Tm^{3+} ions as upconversion optical temperature sensor in the near-infrared region. *Opt. Express* **2017**, *25*, 27845–27856. [CrossRef] [PubMed]
16. García-Rodríguez, L.; de Sousa-Vieira, L.; Hernández-Rodriguez, M.; Lozano-Gorrín, A.; Lavín, V.; Rodríguez-Mendoza, U.; González-Platas, J.; Ríos, S.; Martín, I. Nanoperovskite doped with Yb^{3+} and Tm^{3+} ions used as an optical upconversion temperature sensor. *Opt. Mater.* **2018**, *83*, 187–191. [CrossRef]
17. Hernández-Rodríguez, M.; Lozano-Gorrín, A.; Martín, I.; Rodríguez-Mendoza, U.; Lavín, V. Spectroscopic properties of Nd^{3+} ions in YAP nano-perovskites. *J. Lumin.* **2017**, *188*, 204–208. [CrossRef]
18. Lozano-Gorrín, A.D.; Rodríguez-Mendoza, U.R.; Venkatramu, V.; Monteseguro, V.; Hernández-Rodríguez, M.A.; Martín, I.R.; Lavín, V. Lanthanide-doped $Y3Ga_5O_{12}$ garnets for nanoheating and nanothermometry in the first biological window. *Opt. Mater.* **2018**, *84*, 46–51. [CrossRef]
19. Hernández-Rodríguez, M.A.; Muñoz-Santiuste, J.E.; Lavín, V.; Lozano-Gorrín, A.D.; Rodríguez-Hernández, P.; Muñoz, A.; Venkatramu, V.; Martín, I.R.; Rodríguez-Mendoza, U.R. High pressure luminescence of Nd^{3+} in $YAlO_3$ perovskite nanocrystals: A crystal-field analysis. *J. Chem. Phys.* **2018**, *148*, 044201. [CrossRef]
20. Hernández-Rodríguez, M.; Rodríguez-Mendoza, U.; Lavín, V.; Muñoz-Santiuste, J.; Martín, I.; Lozano-Gorrín, A. High pressure sensitivity of anti-Stokes fluorescence in Nd^{3+} doped yttrium orthoaluminate nano-perovskites. *J. Lumin.* **2018**, *196*, 20–24. [CrossRef]
21. Cai, L.; Nino, J.C. Structure and dielectric properties of Ln $_3NbO_7$ (Ln = Nd, Gd, Dy, Er, Yb and Y). *J. Eur. Ceram. Soc.* **2007**, *27*, 3971–3976. [CrossRef]
22. Abe, R.; Higashi, M.; Sayama, K.; Abe, Y.; Sugihara, H. Photocatalytic Activity of R_3MO_7 and $R_2Ti_2O_7$ (R = Y, Gd, La; M = Nb, Ta) for Water Splitting into H_2 and O_2. *J. Phys. Chem. B* **2006**, *110*, 2219–2226. [CrossRef] [PubMed]
23. Wakeshima, M.; Nishimine, H.; Hinatsu, Y. Crystal structures and magnetic properties of rare earth tantalates RE_3TaO_7(RE = rare earths). *J. Phys. Condens. Matter* **2004**, *16*, 4103–4120. [CrossRef]
24. Lia, Y.; Xub, Q.; Dai, L. A Calcination Technology for Ultrafine La3NbO7 Powder Prepared by Sol-Gel Process. *Adv. Mater. Res.* **2012**, *412*, 271–274. [CrossRef]
25. Preux, N.; Rolle, A.; Merlin, C.; Benamira, M.; Malys, M.; Estournes, C.; Rubbens, A.; Vannier, R.-N. La_3TaO_7 derivatives with Weberite structure type: Possible electrolytes for solid oxide fuel cells and high temperature electrolysers. *Comptes Rendus Chim.* **2010**, *13*, 1351–1358. [CrossRef]
26. Kato, K.; Toyoura, K.; Nakamura, A.; Matsunaga, K. First-principles analysis on proton diffusivity in La_3NbO_7. *Solid State Ionics* **2014**, *262*, 472–475. [CrossRef]
27. Cai, L.; Nino, J.C. Complex ceramic structures. I. Weberites. *Acta Cryst. B* **2009**, *65*, 269–290. [CrossRef]
28. Egaña, A.; Cantelar, E.; Tardío, M.; Muñoz Santiuste, J.E. Synthesis and luminescence properties of Er^{3+} doped La_3NbO_7 ceramic powder. *Opt. Mater.* **2019**, *97*, 109393. [CrossRef]

29. Dai, L.; Xu, Q.; Zhu, S.Z.; Liu, L. Preparation of Ultra–Fine La_3NbO_7 Powder by Solid State Reaction. *Key Eng. Mater.* **2012**, *512–515*, 158–161. [CrossRef]
30. León-Luis, S.F.; Rodriguez-Mendoza, U.; Gonzalez, P.H.; Martin, I.R.; Lavin, V. Role of the host matrix on the thermal sensitivity of Er^{3+} luminescence in optical temperature sensors. *Sens. Actuators B Chem.* **2012**, *174*, 176–186. [CrossRef]
31. León-Luis, S.F.; Rodriguez-Mendoza, U.; Martin, I.R.; Lalla, E.; Lavin, V. Effects of Er^{3+} concentration on thermal sensitivity in optical temperature fluorotellurite glass sensors. *Sens. Actuators B Chem.* **2013**, *176*, 1167–1175. [CrossRef]
32. Venkatramu, V.; León-Luis, S.F.; Rodríguez-Mendoza, U.R.; Monteseguro, V.; Manjón, F.J.; Lozano-Gorrín, A.D.; Valiente, R.; Navarro-Urrios, D.; Jayasankar, C.K.; Muñoz, A.; et al. Synthesis, structure and luminescence of Er^{3+}-doped $Y_3Ga_5O_{12}$ nano-garnets. *J. Mater. Chem.* **2012**, *22*, 13788–13799. [CrossRef]
33. Judd, B.R. Optical Absorption Intensities of Rare-Earth Ions. *Phys. Rev.* **1962**, *127*, 750–761. [CrossRef]
34. Ofelt, G.S. Intensities of Crystal Spectra of Rare-Earth Ions. *J. Chem. Phys.* **1962**, *37*, 511–520. [CrossRef]
35. Brites, C.D.S.; Milla, A.; Carlos, L.D. Lanthanides in Luminescent Thermometry. In *Handbook on the Physics and Chemistry of Rare Earths*; Bünzli, J.V.G., Pecharsky, V.K., Eds.; Elsevier: Amsterdam, The Netherlands, 2016; Volume 49, pp. 339–427.
36. Sung Lim, C.; Aleksandrovsky, A.S.; Molokeev, M.S.; Oreshonkov, A.S.; Atuchin, V. Microwave sol–gel synthesis and upconversion photoluminescence properties of $CaGd_2(WO_4)_4$: Er^{3+}/Yb^{3+} phosphors with incommensurately modulated structure. *J. Solid State Chem.* **2015**, *228*, 160–166.
37. Sung Lim, C.; Aleksandrovsky, A.S.; Molokeev, M.S.; Oreshonkov, A.S.; Atuchin, V.V. Microwave synthesis and spectroscopic properties of ternary scheelite-type molybdate phosphors $NaSrLa(MoO_4)_3$:Er^{3+},Yb^{3+}. *J. Alloys Compd.* **2017**, *713*, 156–163.
38. Peacock, R.D. The Intensities of Lanthanide f-f Transitions. *Struct. Bond.* **1975**, *22*, 83–122.
39. Zhao, H.; Zhang, Z.; Qin, F.; Li, L.; Zheng, Y.; Zhou, Y. Using the upconversion luminescence of the $CaWO_4$:Yb^{3+} − X^{3+} (X = Er/Ho/Tm) phosphors for ratiometric thermal sensing. *J. Lumin.* **2018**, *202*, 301–308.
40. Soni, A.K.; Rai, V.K.; Mahata, M.K. Yb^{3+} sensitized $Na_2Y_2B_2O_7$: Er^{3+} phosphors in enhanced frequency upconversion, temperature sensing and field emission display. *Mater. Res. Bull.* **2017**, *89*, 116–124. [CrossRef]
41. Liu, X.; Lei, R.; Huang, F.; Deng, D.; Wang, H.; Zhao, S.; Xu, S. Dependence of upconversion emission and optical temperature sensing behavior on excitation power in Er^{3+} /Yb^{3+} co-doped BaMoO 4 phosphors. *J. Lumin.* **2019**, *210*, 119–127. [CrossRef]
42. Liu, H.; Zuo, C.; Liu, Y.; Gao, G.; Liu, D.; Wang, T.; Liu, T.; Zhang, Y. Optical thermometry through infrared excited green upconversion of $KLa(MoO_4)_2$:Yb^{3+}/Er^{3+} phosphor. *J. Lumin.* **2019**, *207*, 93–97. [CrossRef]
43. Liu, G.; Wu, L.; Wei, X.; Zhang, D.; Hu, L. Investigation on laser-induced heating in NaYbF4:Er^{3+} for accurate photo-thermal conversion with temperature feedback. *Opt. Commun.* **2018**, *426*, 418–422. [CrossRef]
44. Du, P.; Luo, L.; Li, W.; Yue, Q.; Chen, H. Optical temperature sensor based on upconversion emission in Er-doped ferroelectric $0.5Ba(Zr_{0.2}Ti_{0.8})O_{3-0.5}(Ba_{0.7}Ca_{0.3})TiO_3$ ceramic. *Appl. Phys. Lett.* **2014**, *104*, 2–6. [CrossRef]
45. Suo, H.; Zhao, X.; Zhang, Z.; Shio, R.; Wu, Y.; Xiang, J.; Guo, C. Local Symmetric Distortion Boosted Photon Up-conversion and Thermometric Sensitivity in lanthanum Oxide Nanospheres. *Nanoscale* **2018**, *10*, 9245–9251. [CrossRef]
46. Jin, Y.; Pang, T. Highly efficient green upconversion luminescence of $ZnMoO_4$:$Yb^{3+}/Er^{3+}/Li^{+}$ for accurate temperature sensing. *Spectrochim. Acta Part A Mol. Biomol. Spectrosc.* **2019**, *211*, 306–312. [CrossRef]
47. León-Luis, S.F.; Monteseguro, V.; Rodríguez-Mendoza, U.R.; Rathaiah, M.; Venkatramu, V.; Lozano-Gorrín, A.D.; Valiente, R.; Muñoz, A.; Lavín, V. Optical nanothermometer based on the calibration of the Stokes and upconverted green emissions of Er^{3+} ions in $Y_3Ga_5O_{12}$ nano-garnets. *RSC Adv.* **2014**, *4*, 57691–57701. [CrossRef]
48. Li, L.; Qin, F.; Zhou, Y.; Zheng, Y.; Zhao, H.; Zhang, Z. Temperature sensing based on the 4F7/2/4S3/2−4I15/2 upconversion luminescence intensity ratio in $NaYF_4$:Er^{3+}/Yb^{3+} nanocrystals. *J. Lumin.* **2019**, *206*, 335–341. [CrossRef]
49. Leal, J.J.; Narro-García, R.; Flores-De los Ríos, J.P.; Gutierrez-Mendez, N.; Ramos-Sánchez, V.H.; González-Castillo, J.R.; Rodríguez, E. Effect of TiO_2 on the thermal and optical properties of Er^{3+}/Yb^{3+} co-doped tellurite glasses for optical sensor. *J. Lumin.* **2019**, *208*, 342–349. [CrossRef]
50. Du, P.; Luo, L.; Li, W.; Yue, Q. Upconversion emission in Er-doped and Er/Yb-codoped ferroelectric $Na_{0.5}Bi_{0.5}TiO_3$ and its temperature sensing application. *J. Alloys Compd.* **2014**, *116*, 014102–014107. [CrossRef]
51. Wang, X.; Yan, X. Ultraviolet and infrared photon-excited synergistic effect in Er^{3+-}doped YbF^{3+} phosphors. *Opt. Lett.* **2011**, *36*, 4353–4355. [CrossRef]